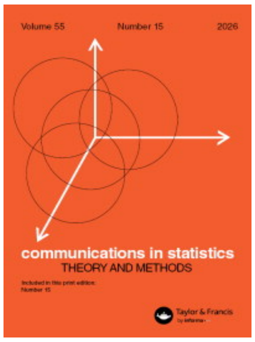

Taylor & Francis
Taylor & Francis Group

Communications in Statistics - Theory and Methods

ISSN: 0361-0926 (Print) 1532-415X (Online) Journal homepage: www.tandfonline.com/journals/lsta20

Modelling covariance structures in determinantal point processes for spatio-temporal interactions

Nafiseh Vafaei, Mari Myllymäki & Mohammad Ghorbani

To cite this article: Nafiseh Vafaei, Mari Myllymäki & Mohammad Ghorbani (2026) Modelling covariance structures in determinantal point processes for spatio-temporal interactions, Communications in Statistics - Theory and Methods, 55:15, 5127-5147, DOI: 10.1080/03610926.2026.2631039

To link to this article: https://doi.org/10.1080/03610926.2026.2631039

Published online: 26 Mar 2026.

COMMUNICATIONS IN STATISTICS—THEORY AND METHODS
2026, VOL. 55, NO. 15, 5127–5147
https://doi.org/10.1080/03610926.2026.2631039

Taylor & Francis
Taylor & Francis Group

OPEN ACCESS

Check for updates

Modelling covariance structures in determinantal point processes for spatio-temporal interactions

Nafiseh Vafaei[a], Mari Myllymäki[b], and Mohammad Ghorbani[c]

[a]Southern Swedish Forest Research Center, Swedish University of Agricultural Sciences, Alnarp, Sweden; [b]Natural Resources Institute Finland (Luke), Helsinki, Finland; [c]Department of Biosystems and Technology, Swedish University of Agricultural Sciences, Alnarp, Sweden

ABSTRACT
Determinantal point processes (dpps) are widely used for modeling repulsive behavior in spatial point patterns, yet their extension to spatio-temporal settings has received little attention. This paper develops a comprehensive framework for spatio-temporal dpps (stdpps) based on covariance and spectral representations. We establish fundamental existence conditions; derive closed-form expressions for first- and second-order summary functions—including the pair correlation function, spectral density, and space–time K-function; and introduce both separable and non separable covariance structures that capture spatial, temporal, and joint space-time inhibition. The theoretical developments are illustrated through simulated examples, which highlight how spatial and temporal range parameters govern the strength and extent of repulsion. Together, these results provide a flexible and computationally tractable framework for modeling regularity in space-time point process data.

ARTICLE HISTORY
Received 7 March 2025
Accepted 6 February 2026

KEYWORDS
Covariance function; regularity; simulation; spatio-temporal point process; spectral density

1. Introduction

Spatio-temporal point processes (STPPs) provide a unified framework for modelling events that occur across space and time, thereby capturing the dependencies between spatial locations and temporal dynamics. Formally, let $X = \{(u_i, t_i)\}_{i=1}^{N} \subseteq W \times [0, T)$, where $W \subseteq \mathbb{R}^d$ is a spatial domain, $T > 0$ is a finite time horizon, and $N \in \mathbb{N}$ denotes the random number of observed events. Although general theory allows $d \geq 1$, in this work we focus on $d = 2$. Thus, X defines a *spatio-temporal point process*, a random collection of events located within the space-time region $W \times [0, T)$. Each event $(u, t) \in X$ corresponds to an occurrence at spatial location $u \in \mathbb{R}^2$ and time $t \in \mathbb{R}$ (Diggle 2007; González et al. 2016). These models have broad applications across various domains, including modelling epidemic outbreaks (Møller and Ghorbani 2012; Diggle 2013; Meyer et al. 2012; Ghorbani et al. 2025), species distributions (Soriano-Redondo et al. 2019; Seaton et al. 2024), and natural disasters (Ogata 1998; Gonzalez et al. 2019; Bernabeu et al. 2024). For a comprehensive overview of the theory and applications of spatio-temporal point processes, see the excellent review by González et al. (2016) and the references therein.

CONTACT Nafiseh Vafaei nafiseh.vafaei@slu.se Southern Swedish Forest Research Center, Swedish University of Agricultural Sciences, Alnarp, Sweden.

Classical Gibbs and Markov point process models have long been employed to represent inhibitory or repulsive interactions between events (e.g., Lieshout 2000; Lieshout and Baddeley 1996; Møller and Waagepetersen 2004). These models are typically defined through probability densities (or equivalently, Papangelou conditional intensities) involving analytically intractable normalizing constants, making the likelihood function analytically unavailable in general (see, e.g., Møller and Waagepetersen 2004, Chapter 7). Consequently, parameter inference often relies on computationally intensive simulation-based methods such as Markov chain Monte Carlo (MCMC) or birth-death Metropolis algorithms rather than direct likelihood-based inference (Lieshout 2000; Møller and Waagepetersen 2004). This computational burden has limited the practical applicability of these models in large-scale spatio-temporal data settings (Møller et al. 1998; Møller and Waagepetersen 2007). These challenges have also hindered the development of spatio-temporal extensions of Gibbs and Markov models; only a few such models have been proposed, for instance, the multi-scale area-interaction model of Iftimi et al. (2018), and spatio-temporal hard-core process of Cronie and Van Lieshout (2015).

Originally introduced by Macchi (1975) as fermion processes, determinantal point processes (DPPs) provide a computationally tractable alternative for modelling repulsive interactions. Defined via the determinant of a matrix based on a kernel function (see Section 2), DPPs exhibit strong repulsion and have been extensively studied in the spatial domain (Lavancier et al. 2015; Biscio and Waagepetersen 2019; Møller et al. 2023). Subsequent research has focused on developing efficient sampling algorithms (Kulesza and Taskar 2012; Affandi et al. 2013; Affandi et al. 2014) and parameter estimation methods (Biscio et al. 2016; Lavancier et al. 2022). Despite these advances, the modelling of *spatio-temporal dependencies* via DPPs remains relatively unexplored. Figure 1 illustrates the difference between two point patterns: one generated from a DPP, which enforces distance-based repulsion and yields a well-dispersed configuration with uniform coverage, and another obtained by independent random sampling from a Poisson point process with the same number of points, which visually exhibits random clustering. We summarize key distinctions among common spatio-temporal point process models in Table 1.

A naive extension of spatial DPPs that simply adds time as an additional dimension fails to capture the intrinsic temporal dynamics often observed in real-world phenomena, such as disease outbreaks, earthquake aftershocks, and network traffic, where past occurrences influence future events. This motivates the development of a framework that explicitly models spatio-temporal interactions rather than treating time as an additional spatial coordinate. The main contributions of this work are as follows: (i) We develop a mathematical framework for DPPs that extends their fundamental properties from purely spatial to spatio-temporal domains; (ii) We introduce valid covariance structures that capture both spatial and temporal repulsion while ensuring positive semi-definiteness; (iii) through an extensive simulation study and theoretical explanation, we demonstrate the practical use of these models. For convenience, we refer to this spatio-temporal extension of DPPs as the STDPP framework. By incorporating a temporal kernel, STDPPs overcome key limitations of spatial DPPs, enabling more accurate modelling and prediction of event occurrences over space and time. The proposed framework provides a powerful tool for analyzing complex event dynamics in real-world datasets. For example, accurately modelling the spread of epidemics requires accounting for both geographic dispersion and temporal progression, dependencies that traditional Markov models often struggle to capture efficiently.

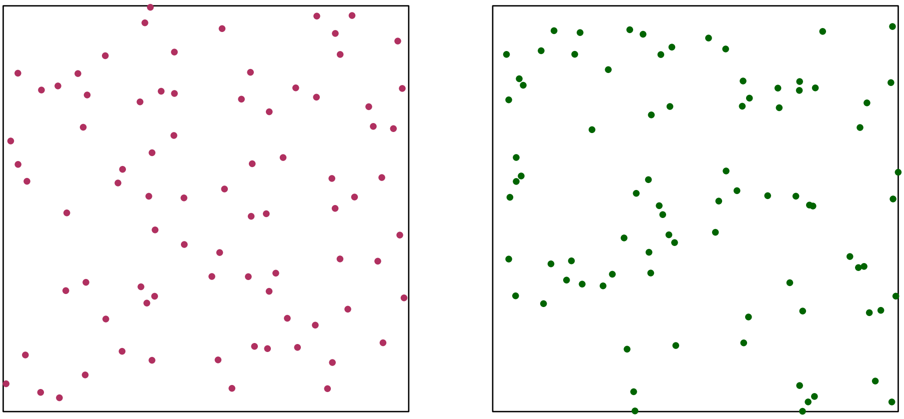

Figure 1. Comparison of two point patterns: (Left) a spatial realization from a dpp showing repulsive behavior, and (Right) a realization from a Poisson point process conditioned on the same number of points, exhibiting random clustering.

Table 1. Comparison of common spatio-temporal point process models.

Model	Interaction Type	Tractability	Simulation	Inference
Gibbs / Markov	Repulsive or attractive	Intractable likelihood	MCMC	Computationally heavy
LGCP	Clustered (attractive)	Log-Gaussian structure	Fast	High variability
stdpp	Repulsive	Closed-form covariance	Exact thinning	Efficient

2. Basic concepts and statistical properties

Let X be a spatio-temporal point process in the planar setting, that is, $X \subseteq \mathbb{R}^2 \times \mathbb{R}$. Assume that X admits nth-order product densities $\rho^{(n)}$ $(n \geq 1)$, which describes the frequency of configurations of n events in space–time. Let $B_1, \ldots, B_n$ be pairwise disjoint infinitesimal space-time regions with infinitesimal volumes $\mathrm{d}V_1, \ldots, \mathrm{d}V_n$, each containing an event (u_i, t_i), $i = 1, \ldots n$. Then,

$$\rho^{(n)}\big((u_1, t_1), \ldots, (u_n, t_n)\big)\mathrm{d}V_1 \cdots \mathrm{d}V_n$$

is the probability that X places exactly one event in each of the regions $B_1, \ldots, B_n$. More formally, for any Borel sets $B_1, \ldots, B_n \subseteq \mathbb{R}^2 \times \mathbb{R}$, the expected number of ordered n-tuples of distinct events of X falling in $B_1 \times \cdots \times B_n$ is

$$\mathbb{E}\Big[\sum_{\substack{\big((u_1,t_1)\ldots,(u_n,t_n)\big)\in X \\ (u_i,t_i)\neq(u_j,t_j)\ \forall i\neq j}} \prod_{i=1}^{n} \mathbf{1}_{B_i}\big((u_i, t_i)\big)\Big]$$
$$= \int_{B_1} \cdots \int_{B_n} \rho^{(n)}\big((u_1, t_1)\ldots, (u_n, t_n)\big)\, \mathrm{d}(u_1, t_1) \cdots \mathrm{d}(u_n, t_n),$$

where each point $(u_i, t_i) \in \mathbb{R}^2 \times \mathbb{R}$ denotes an event's spatial and temporal coordinates (Daley and Vere-Jones 2008; Cronie and Van Lieshout 2015; Iftimi:etal:18).

Definition 1. *Let C be a kernel function from $(\mathbb{R}^2 \times \mathbb{R}) \times (\mathbb{R}^2 \times \mathbb{R})$ to $\mathbb{R}$. A spatio-temporal point process X is called a Spatio-Temporal Determinantal Point Process (STDPP) with kernel function C, written $X \sim$ STDPP(C), if its nth-order product density is given by*

$$\rho^{(n)}\big((u_1, t_1), \ldots, (u_n, t_n)\big) = \det\big\{C\big((u_i, t_i), (u_j, t_j)\big)\big\}_{1 \le i,j \le n},$$

for $(u_i, t_i) \in (\mathbb{R}^2 \times \mathbb{R})$ and $n = 1, 2, \ldots$. Here, $\{C((u_i, t_i), (u_j, t_j))\}_{1 \le i,j \le n}$ denotes the $n \times n$ matrix with entries $C((u_i, t_i), (u_j, t_j))$, and $\det\{A\}$ denotes the determinant of the matrix A.

A Poisson process with intensity function $\rho(u, t)$ emerges as a special case of STDPP(C) when

$$C\big((u, t), (u, t)\big) = \rho(u, t), \quad \text{and} \quad C\big((u, s), (v, t)\big) = 0 \text{ if } u \neq v \text{ or } s \neq t.$$

In this case the kernel matrix is diagonal, so its determinant reduces to the product of its diagonal entries, and the points of X are independent.

In general, a point process X is well-defined only when its product densities are non negative for all configurations of n points, that is,

$$\rho^{(n)}\big((u_1, t_1), \ldots, (u_n, t_n)\big) \ge 0 \quad \text{for all } \big\{(u_i, t_i)\big\}_{i=1}^{n},$$

which can be viewed as the joint intensity function describing the likelihood of observing n points at specific space–time locations. This fundamental requirement guarantees that the associated probability density is well-defined and non negative. For a STDPP as in Definition 1, this requirement is satisfied whenever the Gram matrix

$$\mathbf{C} = \Big\{C\big((u_i, t_i), (u_j, t_j)\big)\Big\}_{1 \le i,j \le n}$$

is positive semi-definite for every finite configuration $\{(u_1, t_1), \ldots, (u_n, t_n)\}$. Indeed, for Hermitian positive semi-definite matrices, the determinant equals the product of non negative eigenvalues (see, e.g., Strang 2006; Horn and Johnson 2013; Adachi 2020), and hence $\rho^{(n)}(x_1, \ldots, x_n) = \det(\mathbf{C}) \ge 0$. Thus, any valid covariance function–i.e., any kernel that yields positive semi-definite Gram matrices–is an admissible choice for constructing a STDPP. This condition is analogous to the positive semi-definiteness requirement for covariance functions in Gaussian process theory and plays the same foundational role in ensuring probabilistic coherence and numerical stability of the STDPP framework.

A further necessary condition for the existence of a STDPP(C) is that all eigenvalues $\{\lambda_\ell\}_{\ell \ge 1}$ of the associated integral operator satisfy $0 \le \lambda_\ell \le 1$, $\ell = 1, 2, \ldots$, which is the natural spatio-temporal extension of the classical DPP spectral condition (Lavancier et al. 2015) This condition guarantees that the Fredholm determinant $\det(I - \mathbf{C}_A)$ (Borodin et al. 2019), that defines the void probability $\mathbb{P}(X(A) = 0)$, remains within $[0, 1]$ for any bounded region A, where $\mathbf{C}_A$ is the restriction of $\mathbf{C}$ to $A \times A$. Eigenvalues outside this range would lead to invalid (negative or greater-than-one) probabilities, violating measure consistency. Intuitively, each eigenvalue λ_ℓ quantifies the *repulsion strength* or *occupancy level* of the process along orthogonal spatial–temporal modes. Each eigenfunction of $\mathbf{C}$ represents an independent mode of variation in the underlying space-time field, and its associated eigenvalue acts as a weight determining how likely this mode is "occupied" by a point. When $\lambda_\ell = 1$, the corresponding mode is fully occupied, implying perfect exclusion in that component, no two points can simultaneously occur in that mode. When $0 < \lambda_\ell < 1$, the mode is only partially occupied, allowing some proximity between events. Values $\lambda_\ell > 1$ would imply "over-occupation," which would force the determinant, and hence the corresponding probability, to become negative, an impossibility. Hence, the spectral bound $0 \le \lambda_\ell \le 1$ is both necessary and sufficient for the existence of a determinantal point process with kernel C.

As previously mentioned, any *valid covariance function* that produces a positive semi-definite matrix is an admissible choice for the kernel C. The structure of this covariance function plays a critical role in capturing the underlying space–time interactions. In this study, we consider two main classes of covariance models:

- *Separable models*, where the kernel factorizes into independent spatial and temporal components. These models simplify computation but can limit flexibility in representing complex dependencies (see details in Section 3.2).
- *Non separable models*, where spatial and temporal interactions are coupled, allowing more realistic modelling of space–time dynamics at the expense of increased computational complexity (details explained in Section 3.3).

By leveraging the spectral properties of DPP kernels, the proposed approach preserves computational efficiency while extending applicability to space-time point pattern data. The STDPP framework thus provides a scalable and interpretable model for repulsive event interactions evolving across space and time.

2.1. First- and second-order characteristics

By Definition 1, the moment characteristics of arbitrary order n ($n \ge 1$) follow directly. The first-order intensity function is

$$\rho(u,t) = C((u,t),(u,t))$$

and the second-order product density, which describes the interaction between two points, is

$$\rho^{(2)}((u_1,t_1),(u_2,t_2)) = C((u_1,t_1),(u_1,t_1))C((u_2,t_2),(u_2,t_2)) - |C((u_1,t_1),(u_2,t_2))|^2.$$

To jointly model spatial and temporal dependencies, we consider kernels of the form

$$C\big((u_1,t_1),(u_2,t_2)\big) = \sqrt{\rho(u_1,t_1)}\, R\left(\frac{(u_1,t_1)}{\alpha_s}, \frac{(u_2,t_2)}{\alpha_t}\right) \sqrt{\rho(u_2,t_2)}, \tag{1}$$

where $R(\cdot,\cdot)$ is a valid space–time correlation function. The parameters $\alpha_s > 0$ and $\alpha_t > 0$ are the spatial and temporal scale parameters, respectively, and control the corresponding correlation ranges. The intensity function $\rho(u,t)$ specifies the inhomogeneous first-order structure. This parametrization makes explicit that spatial and temporal components are scaled independently: α_s affects only spatial distances, whereas α_t governs temporal lags. The model accommodates both homogeneous and inhomogeneous settings, and the correlation function $R(\cdot,\cdot)$ may be chosen as either separable or non separable, as described in Sections 3.2–3.3. The *inhomogeneous space-time pair correlation function* is then given by

$$\begin{aligned} g\big((u_1,t_1),(u_2,t_2)\big) &= \frac{\rho^{(2)}\big((u_1,t_1),(u_2,t_2)\big)}{\rho(u_1,t_1)\rho(u_2,t_2)} \\ &= 1 - \Big|R((u_1,t_1)/\alpha_s,(u_2,t_2)/\alpha_t)\Big|^2 \le 1. \end{aligned} \tag{2}$$

Since $g((u_1,t_1),(u_2,t_2)) \le 1$ for all distinct points, the process exhibits repulsive interaction, a hallmark of regular point patterns (Møller and Waagepetersen 2004; Illian et al. 2008; Gabriel 2014). Smaller values of g (closer to zero) indicate stronger repulsion, whereas values closer to one correspond to weaker interaction, approaching Poisson behavior.

2.2. Second-order intensity reweighted stationarity

A spatio-temporal point process X is said to be *second-order intensity reweighted stationary* (SOIRS) if its pair correlation function depends only on spatial and temporal lags, that is,

$$g\big((u_1,t_1),(u_2,t_2)\big) = g_0(u_2-u_1,\ t_2-t_1)$$

for some function g_0 (see, e.g., Baddeley et al. 2000; Ghorbani 2013). SOIRS does not require a constant intensity; only the *reweighted second-order structure* is translation invariant.

For a STDPP with kernel of the form (1), (2) implies that SOIRS holds whenever

$$R\big((u_1,t_1)/\alpha_s,(u_2,t_2)/\alpha_t\big) = R_0\left(\frac{\|u_2-u_1\|}{\alpha_s},\ \frac{|t_2-t_1|}{\alpha_t}\right),$$

for some correlation function R_0 with $R_0(0,0)=1$. When, in addition to SOIRS, the process is *stationary* so that $\rho(u,t)\equiv\rho$ is constant, the kernel form (1) implies that

$$\rho = C(0,0) = \rho\, R_0(0,0).$$

Because any valid correlation function satisfies $R_0(0,0)=1$, the intensity is indeed given by the kernel evaluated at zero spatial and temporal lags. Thus, in the stationary case, the kernel simultaneously determines both the marginal intensity and the second-order dependence structure, in direct analogy with the variance–covariance link in second-order stationary random fields. The normalization $R_0(0,0)=1$ ensures that the correlation attains its maximum at zero lag, and that the decay of R_0 governs how repulsion weakens across space and time. If, in addition, R_0 is isotropic in space, then the pair correlation function (2) depends only on the spatial distance $r=\|u_2-u_1\|$ and the temporal lag $s=|t_2-t_1|$, yielding

$$g(r,s) = 1 - \big|R_0(r/\alpha_s,\ s/\alpha_t)\big|^2. \tag{3}$$

Repulsion weakens as either r or s increases, and the process approaches independence as $R_0\to 0$. We refer to (r_0,s_0) as a correlation range if $g(r,s)\approx 1$ whenever $r>r_0$ or $s>s_0$.

For a SOIRS, spatially isotropic, and constant-intensity process, the space–time K-function (Gabriel and Diggle 2009; Møller and Ghorbani 2012) is

$$K(r,s) = 2\pi\int_0^r\int_0^s g(u,t)\,u\,\mathrm{d}u\,\mathrm{d}t,$$

where g is given by (3). Substitution of (3) yields

$$K(r,s) = \pi r^2 s - \int_0^r\int_0^s \big|R_0(u/\alpha_s,\ t/\alpha_t)\big|^2\,u\,\mathrm{d}u\,\mathrm{d}t. \tag{4}$$

Under these assumptions, the stationary space-time g- and K-functions coincide with their classical forms.

3. Examples of spatio-temporal determinantal point processes

This section develops a family of stationary spatio-temporal covariance structures suitable for constructing valid STDPPs. The exposition is organized around the spectral representation of covariance functions, which provides a natural and analytically tractable route for verifying the existence condition of STDPPs. In particular, the requirement that the spectral density satisfies $\varphi(\omega,\tau)\le 1$ guarantees that the associated covariance operator has eigenvalues in $[0,1]$, thereby yielding a valid STDPP. Section 3.1 reviews the covariance–spectral duality, which forms the mathematical foundation for constructing space–time kernels. Sections 3.2 and 3.3 develop separable and non separable covariance models by employing the Fourier transform of positive finite measures–known as spectral measures, motivated by their interpretability and their ability to encode different forms of space–time repulsion.

3.1. The covariance function and its spectral density

For a stationary spatio-temporal random field, the covariance function may be expressed as the Fourier transform of a positive finite measure, establishing a fundamental link between spatial–temporal dependence and its spectral representation. According to the Wiener-Khintchine theorem (see, e.g., Rasmussen and Williams 2006), if the spectral density function $\varphi(\cdot,\cdot)$ exists, the covariance function $C(\cdot,\cdot)$ and the spectral density $\varphi(\cdot,\cdot)$ are Fourier duals, given by

$$C(r,s) = \int_{\mathbb{R}^{d+1}} e^{2\pi i(\omega^T r+\tau s)}\varphi(\omega,\tau)\mathrm{d}\omega\mathrm{d}\tau,$$
$$\varphi(\omega,\tau) = \int_{\mathbb{R}^{d+1}} e^{-2\pi i(\omega^T r+\tau s)}C(r,s)\mathrm{d}r\mathrm{d}s, \tag{5}$$

where $\omega \in \mathbb{R}^d$ is the spatial frequency and $\omega^T u$ denotes their inner product, and τ denotes the temporal frequency. This duality provides a powerful characterization of the dependence structure: the covariance function describes local interactions in space and time, while its spectral density captures the same information in the frequency domain.

For a STDPP with kernel C, the spectral density must satisfy

$$\varphi(\omega,\tau) \leq 1, \qquad \text{for all } (\omega,\tau) \in \mathbb{R}^d \times \mathbb{R} \tag{6}$$

which is the spatio-temporal extension of Proposition 3.1 in Lavancier et al.(2015). Condition (6) is the frequency-domain analogue of the eigenvalue constraint $0 \leq \lambda_\ell \leq 1$ for the finite-dimensional Gram matrices introduced in Section 2, thereby guaranteeing that all determinants defining product densities are non negative. Intuitively, $\varphi(\omega,\tau)$ measures how strongly the process "occupies" the spatio-temporal frequency (ω,τ): $\varphi(\omega,\tau) = 1$ correspond to a fully occupied mode (maximal repulsion), $\varphi(\omega,\tau) = 0$ to an unoccupied mode (no contribution). The upper bound 1 prevents over-occupation and thus preserves the repulsive nature of STDPPS.

3.2. Separable spatio-temporal covariance function

A widely used class of space–time covariance functions is the *separable class*, for which spatial and temporal dependence factorize. A separable kernel can be written as

$$C_{\text{sep}}(r,s) = C_0^s(r)\, C_0^t(s), \tag{7}$$

where C_0^s and C_0^t are valid spatial and temporal covariance functions. This form offers substantial analytical and computational advantages: positive definiteness follows directly from the validity of the marginal covariance functions, and spectral calculations become tractable. The corresponding spectral density has the product structure

$$\varphi_{\text{sep}}(\omega,\tau) = \left[\int_{\mathbb{R}^d} e^{-2\pi i\omega^T u}C_0^s(r)\mathrm{d}r\right] \times \left[\int_{\mathbb{R}} e^{-2\pi i\tau t}C_0^t(s)\mathrm{d}s\right] = \varphi_0^s(\omega)\varphi_0^t(\tau),$$

where $\varphi_0^s(\omega)$ and $\varphi_0^t(\tau)$ are the spatial and temporal spectral densities, respectively. Using the existence condition (6), a STDPP with kernel (7) exists whenever $\varphi_0^s(\omega)\varphi_0^t(\tau) \leq 1$, for all (ω, τ).

For this class of kernels, the pair correlation function,based on formula (2), takes the simple form

$$g(r,s) = 1 - \left|R_0^s(r/\alpha_s)\right|^2 \left|R_0^t(s/\alpha_t)\right|^2, \tag{8}$$

where R_0^s and R_0^t are the correlation functions in space and time and $\alpha_s, \alpha_t > 0$ are spatial and temporal scale parameters, respectively. The associated K-function derived using formula (4) is given by

$$K(r,s) = \pi r^2 s - \int_0^r u\left|R_0^s(u/\alpha_s)\right|^2 \mathrm{d}u \int_0^s \left|R_0^t(t/\alpha_t)\right|^2 \mathrm{d}t. \tag{9}$$

3.2.1. Gaussian-exponential stdpp *model:*

A wide range of valid spatial and temporal covariance models have been proposed in the literature, including the Matérn, power-exponential, and Gaussian classes (see, e.g., Matérn 1960; Cressie 1993; Cressie and Wikle 2011). As an illustrative example, we consider the *Gaussian covariance function*

$$C_0^s(u) = \sqrt{\rho}\exp(-\|u\|^2/\alpha_s^2), \quad u \in \mathbb{R}^2,$$

with spectral density $\varphi_0^s(\omega) = \sqrt{\rho}\pi\alpha_s^2\exp(-\pi^2\alpha_s^2\|\omega\|^2)$ for spatial component, and the *exponential covariance function*

$$C_0^t(t) = \sqrt{\rho}\exp(-|t|/\alpha_t), \quad t \in \mathbb{R},$$

with spectral density $\varphi_0^t(\tau) = (2\sqrt{\rho}\alpha_t)/(1 + 4\pi^2\alpha_t^2|\tau|^2)$ for temporal. Here $\alpha_s > 0$ and $\alpha_t > 0$ are the spatial and temporal range parameters, respectively. Note that $C(0,0) = \rho$. Thus, with these choices, a stationary STDPP with intensity ρ and the separable covariance function

$$C_{\text{sep}}(u,t) = \rho\exp\left(-\frac{\|u\|^2}{\alpha_s^2} - \frac{|t|}{\alpha_t}\right) \tag{10}$$

will exist if

$$\varphi_{\text{sep}}(\omega,\tau) = \frac{2\pi\rho\alpha_s^2\alpha_t}{(1 + 4\pi^2\alpha_t^2\tau^2)}\exp\left(-\pi^2\alpha_s^2\|\omega\|^2\right) < 1. \tag{11}$$

We call this model *Gaussian-exponential STDPP model* and denote it by STDPP(C_{sep}). Since the maximum of the spectral density occurs at $(0,0)$, thus the existence of a STDPP(C_{sep}) simplifies to $\rho \leq (2\pi\alpha_s^2\alpha_t)^{-1}$, hence the maximal admissible intensity is $\rho_{\max} = (2\pi\alpha_s^2\alpha_t)^{-1}$. Using (8), for this process the pair correlation function is simply given by

$$g(r,s) = 1 - \exp\left(-\frac{2r^2}{\alpha_s^2} - \frac{2s}{\alpha_t}\right) \tag{12}$$

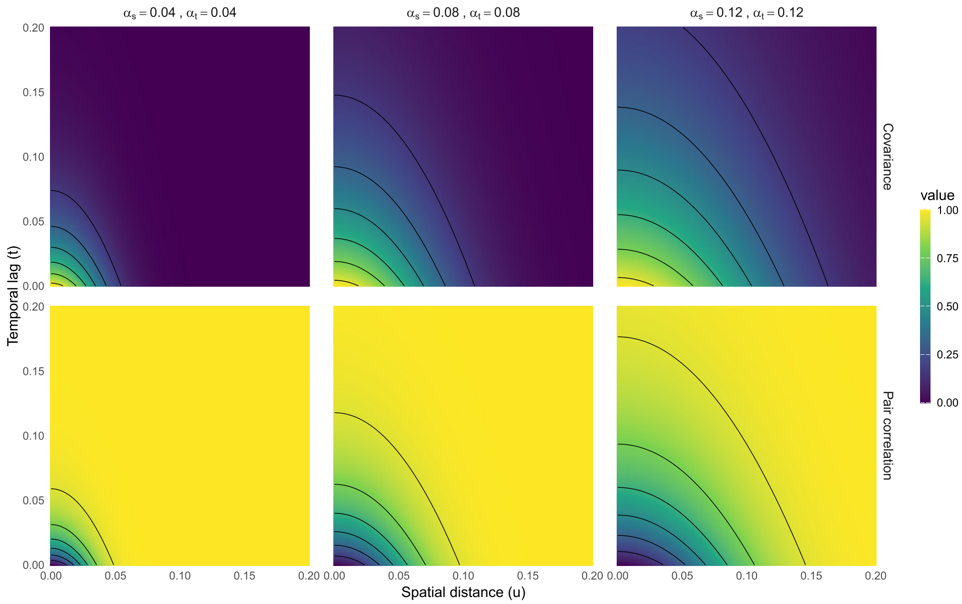

Figure 2. Theoretical covariance function (top row) and pair correlation function (bottom row) for the **Gaussian-exponential**stdpp model. Each column corresponds to a different combination of spatial and temporal range parameters (α_s, α_t), chosen so that the model is admissible for an intensity $\rho = 90$. The results illustrate how increasing spatial and temporal ranges extends the range of interaction and enhances the strength of repulsion.

and the corresponding K-function, obtained from (9), is given by the following closed-form expression

$$K(r,s) = \pi r^2 s - \int_0^r \int_0^s \exp\left(\frac{-2u^2}{\alpha_s^2} - \frac{2t}{\alpha_t}\right) u\mathrm{d}u\mathrm{d}t$$
$$= \pi r^2 s - \frac{\alpha_s^2 \alpha_t}{8}\left(1 - e^{-2r^2/\alpha_s^2}\right)\left(1 - e^{-2s/\alpha_t}\right). \tag{13}$$

The covariance function in (10) is strictly increasing in the spatial and temporal range parameters α_s and α_t for any fixed $(u, t) \neq (0, 0)$. Increasing either parameter slows the decay of spatio-temporal correlation, indicating that events remain correlated across larger spatial distances and longer temporal lags. This behavior is clearly visible in Figure 2 (top row), where the covariance surfaces broaden as α_s and α_t grow, confirming their interpretation as spatial and temporal range parameters.

In contrast, the pair correlation function in (12) decreases monotonically with both α_s and α_t for any fixed $(r, s) \neq (0, 0)$. Analytically, the partial derivatives of $g(r, s)$ with respect to α_s and α_t are strictly negative, demonstrating that larger range parameters reduce $g(r, s)$ and thus strengthen inhibition. This pattern is visually confirmed in Figure 2 (bottom row), where increasing α_s or α_t lowers the values of $g(r, s)$ and expands the region of repulsion. Thus, α_s and α_t govern the spatial and temporal scales of dependence: small values produce short-range, localized repulsion, whereas larger values yield broader, longer-lasting inhibition across space and time.

3.3. Non separable spatio-temporal covariance function

While separable models are analytically convenient, many real processes exhibit joint spatial–temporal dependence that cannot be factorized into purely spatial and purely temporal components. Following Fuentes et al. (2007), we consider a flexible class of non separable spatio-temporal spectral densities of the form

$$\varphi_\epsilon(\omega,\tau) = \gamma\left(\alpha_s^2\alpha_t^2 + \alpha_t^2\|\omega\|^2 + \alpha_s^2\tau^2 + \epsilon\|\omega\|^2\tau^2\right)^{-\nu}. \tag{14}$$

which generalizes the widely used Matérn-type spectral densities used in spatial statistics (Cressie and Wikle 2011). The non negative parameter α_s^{-1} (spatial range) governs the rate of the spatial correlation decay, while the non negative parameter α_t^{-1} (temporal scale) controls the decay rate for temporal correlation, and $\gamma > 0$ is a scale parameter. The smoothness parameter ν determines the differentiability of the process and must satisfy $\nu > (d+1)/2$ for the spectral density to be finite. The interaction between spatial and temporal components is governed by ϵ: the model is strictly non separable for $0 \le \epsilon < 1$ and becomes separable when $\epsilon = 1$. The maximum of the spectral density φ_ϵ occurs at $(\omega,\tau) = (0,0)$ and equals $\gamma(\alpha_s^2\alpha_t^2)^{-\nu}$; hence, a STDPP with spectral density (14) exists if $\gamma < \left(\alpha_s^2\alpha_t^2\right)^\nu$.

3.3.1. Separable Matérn STDPP model:

In the separable case, i.e., when $\epsilon = 1$, the spectral density factorizes as

$$\varphi_{\epsilon=1}(\omega,\tau) = \gamma\left(\alpha_s^2 + \|\omega\|^2\right)^{-\nu}\left(\alpha_t^2 + \tau^2\right)^{-\nu} = \varphi_{\mathrm{M}}^s(\omega)\varphi_{\mathrm{M}}^t(\tau), \tag{15}$$

where $\varphi_{\mathrm{M}}^s(\omega)$ and $\varphi_{\mathrm{M}}^t(\tau)$ are *Matérn-type spectral densities* in space and time, respectively. By applying the Fourier inversion formula (5) and using the formulas 6.726.4 and 8.432.5 in Gradshteyn and Ryzhik (2007) with $d = 2$, the corresponding separable spatio-temporal covariance function is

$$\begin{aligned} C_{\epsilon=1}(u,t) = {} & \frac{4\gamma\pi\sqrt{\pi}}{2^{2\nu-1/2}(\Gamma(\nu))^2}\left(\frac{2\pi|t|}{\alpha_t}\right)^{\nu-1/2}\left(\frac{2\pi\|u\|}{\alpha_s}\right)^{\nu-1} \\ & \times \mathcal{K}_{\nu-\frac{1}{2}}\Big(2\pi\alpha_t|t|\Big)\mathcal{K}_{\nu-1}\Big(2\pi\alpha_s\|u\|\Big), \end{aligned}$$

where $\mathcal{K}_\nu(\cdot)$ is the modified Bessel function of the second kind of order ν. The spatio-temporal covariance $C_{\epsilon=1}(u,t)$ is thus equal to the product of Matérn covariance functions in space and time. We refer to the STDPP model generated by $C_{\epsilon=1}$ as the *separable Matérn STDPP* model, denoted by STDPP($C_{\epsilon=1}$). Using the special cases, $\mathcal{K}_{\frac{1}{2}}(x) = e^{-x}(2x/\pi)^{-1/2}$ and $\mathcal{K}_{\frac{3}{2}}(x) = e^{-x}(1+x^{-1})(2x/\pi)^{-1/2}$ (Abramowitz and Stegun 1992), the above covariance function for $\nu = 2$ simplifies to

$$C_{\epsilon=1}(u,t) = \frac{\gamma\pi^2}{4\alpha_s^2\alpha_t^3}\big[(2\pi\alpha_t|t|+1)\exp(-2\pi\alpha_t|t|)\big]\big[(2\pi\alpha_s\|u\|)\mathcal{K}_1(2\pi\alpha_s\|u\|)\big]. \tag{16}$$

For this case, using the property $\lim_{x\to 0} x\mathcal{K}_1(x) = 1$ (Yang and Chu 2017), the intensity of the process is $\rho = C_{\epsilon=1}(0,0) = (\gamma\pi^2)/(4\alpha_s^2\alpha_t^3)$. Since $\gamma < \alpha_s^4\alpha_t^4$, a STDPP with kernel (16) exists if $4\rho \le \pi^2\alpha_s^2\alpha_t$. For this separable case with $\epsilon = 1$, the pair correlation function, using (3), is given by

$$g(r,s) = 1 - \Big[(2\pi\alpha_t s+1)^2\exp(-4\pi\alpha_t s)\Big]\Big[(2\pi\alpha_s r)\mathcal{K}_1(2\pi\alpha_s r)\Big]^2, \tag{17}$$

and the corresponding K-function is

$$K(r,s) = \pi r^2 s - \frac{\pi \alpha_s r^4}{6\alpha_t} A(s)\, B(r), \tag{18}$$

where

$$B(r) \;=\; \mathcal{K}_1(2\pi\alpha_s r)^2 - \mathcal{K}_0(2\pi\alpha_s r)\,\mathcal{K}_2(2\pi\alpha_s r),$$

and

$$A(s) \;=\; \frac{7}{2} - e^{-4\pi\alpha_t s}\big(3 + 8\pi\alpha_t s + 8\pi^2\alpha_t^2 s^2\big).$$

For the separable Matérn model, the covariance function in (16) decreases monotonically with the spatial and temporal scale parameters α_s and α_t for any fixed $(u,t) \neq (0,0)$, and therefore increases with their inverses α_s^{-1} and α_t^{-1}. So, under this parameterization, the spatial and temporal range parameters are α_s^{-1} and α_t^{-1}. Larger values of these range parameters correspond to a slower decay of the covariance function, producing longer-range spatial and temporal dependence. This behavior is clearly visible in Figure 3 (top row), where the covariance surfaces become broader as α_s^{-1} and α_t^{-1} increase. In contrast, the pair correlation function in (17) exhibits the opposite behavior. Since $g(r,s)$ increases with α_s and α_t, larger scale parameters (i.e., shorter ranges) yield weaker inhibition, with $g(r,s)$ approaching 1 more rapidly. Conversely, increasing the range parameters α_s^{-1} and α_t^{-1} leads to stronger and more persistent repulsion. This is illustrated in Figure 3 (bottom row), where the region in which $g(r,s) < 1$, expands as the range parameters grow, indicating that inhibition extends over greater spatial and temporal scales.

3.3.2. Non separable Matérn stdpp *model:*

For $\epsilon \in (0,1)$ the spatio-temporal covariance function corresponding to (14) does not admit a simple closed-form expression and must be computed numerically. For the case $\epsilon = 0$, the stationary non separable spatio-temporal spectral density is given by

$$\varphi_{\epsilon=0}(\omega,\tau) = \gamma\left(\alpha_s^2\alpha_t^2 + \alpha_t^2|\omega|^2 + \alpha_s^2\tau^2\right)^{-\nu}, \tag{19}$$

which is non separable but still admits an explicit covariance function. Combining (5) and (19), and applying formulas 6.726.4 and 8.432.5 in Gradshteyn and Ryzhik (2007), the covariance function for general d is

$$C_0(u,t) = \frac{\gamma\pi^{\frac{d+1}{2}}}{2^{\nu-\frac{d+1}{2}}\Gamma(\nu)\alpha_s^{(2\nu-d)}\alpha_t^{(2\nu-1)}}\left\{2\pi\alpha_s\Big(\big(\frac{\alpha_t}{\alpha_s}t\big)^2 + \|u\|^2\Big)^{1/2}\right\}^{\nu-\frac{d+1}{2}}$$
$$\times\, \mathcal{K}_{\nu-\frac{d+1}{2}}\left(2\pi\alpha_s\Big(\big(\frac{\alpha_t}{\alpha_s}t\big)^2 + \|u\|^2\Big)^{1/2}\right),$$

where $\mathcal{K}_\nu$ denotes the modified Bessel function of the second kind. According to (6), for $d = 2$ and $\nu = 2$, there exists a STDPP with kernel

$$C_0(u,t) = \frac{\gamma\pi^2}{2\alpha_s^2\alpha_t^3}\exp\left(-2\pi\left(\alpha_t^2|t|^2 + \alpha_s^2\|u\|^2\right)^{1/2}\right) \tag{20}$$

if and only if $\gamma < \alpha_s^4\alpha_t^4$. Further, it follows that for this covariance functions, the intensity is $\rho = C_0(0,0) = (\gamma\pi^2)/(2\alpha_s^2\alpha_t^3)$. Thus, under the condition $\gamma < \alpha_s^4\alpha_t^4$, it holds that $2\rho \leq$

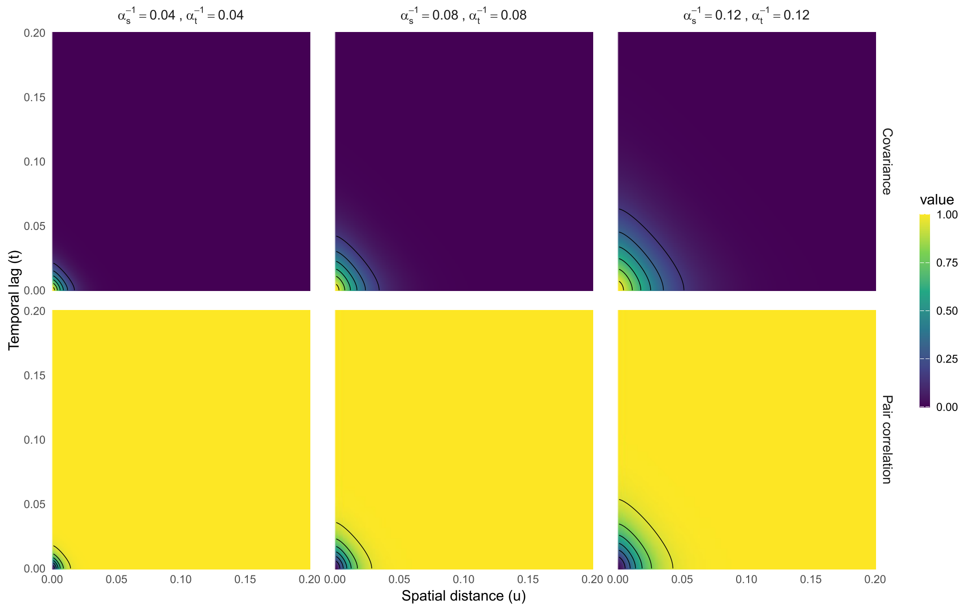

Figure 3. Theoretical covariance (top row) and pair correlation (bottom row) functions for the **separable Matérn**stdpp model. Each column corresponds to a different combination of spatial and temporal range parameters $(\alpha_s^{-1}, \alpha_t^{-1})$ selected in accordance with the existence condition assuming $\rho_{\max} = 90$. The results demonstrate that increasing α_s^{-1} and α_t^{-1} extends the range of interaction and enhances the strength of repulsion.

$\pi^2\alpha_s^2\alpha_t$. Therefore, for a STDPP with the above covariance function, the intensity should be at most $\rho_{\max} = \pi^2\alpha_s^2\alpha_t/2$.

For this process the pair correlation function is simply given by

$$g(r, s) = 1 - \exp\left(-4\pi\sqrt{\alpha_t^2 s^2 + \alpha_s^2 r^2}\right), \qquad r \geq 0,\ s \geq 0. \tag{21}$$

since $C_0(u, t) = \rho\ \exp(-2\pi\sqrt{\alpha_t^2 t^2 + \alpha_s^2\|u\|^2})$ implies $g = 1 - |C_0|^2/\rho^2$ for a stationary STDPP with kernel C_0. Employing the general definition of the space–time K-function (4), the K-function corresponding to the covariance model (20) and the pair correlation function (21) is obtained as

$$\begin{aligned} K(r, s) &= 2\pi \int_0^r \int_0^s g(u, t)\, u\, \mathrm{d}t\, \mathrm{d}u \\ &= 2\pi \int_0^r \int_0^s \left[1 - \exp\big(-4\pi\sqrt{\alpha_t^2 t^2 + \alpha_s^2 u^2}\big)\right] u\, \mathrm{d}t\, \mathrm{d}u \\ &= \pi r^2 s - 2\pi \int_0^r \int_0^s \exp\big(-4\pi\sqrt{\alpha_t^2 t^2 + \alpha_s^2 u^2}\big)\, u\, \mathrm{d}t\, \mathrm{d}u. \end{aligned} \tag{22}$$

The second term in (22) does not have a closed-form expression in elementary functions; in practice, it can be evaluated numerically. However, it can be expressed in terms of an *incomplete modified Bessel function of the second kind*, denoted by $\mathcal{J}_1$, following Jones (2007):

$$K(r, s) = \pi r^2 s - \frac{2\pi}{\alpha_t^2} \int_0^r u\, \mathcal{J}_1\left(4\pi\alpha_s u,\ 4\pi\sqrt{\alpha_s^2 u^2 + \alpha_t^2 s^2}\right) \mathrm{d}u, \tag{23}$$

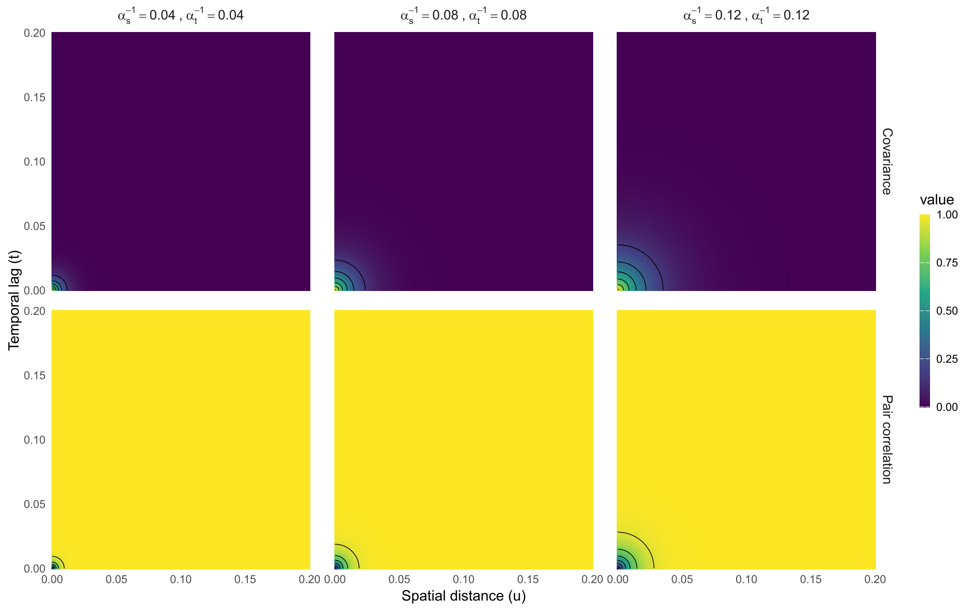

Figure 4. Theoretical covariance (top row) and pair correlation (bottom row) functions for the **non separable Matérn**stdpp model. Each column corresponds to a different combination of the parameters $(\alpha_s^{-1}, \alpha_t^{-1})$ selected according to the existence condition assuming $\rho_{\max} = 90$. This illustrates how increasing α_s^{-1} and α_t^{-1} broadens the effective interaction range and intensifies the repulsive behavior.

where

$$\mathcal{J}_1(a,b) = \int_a^b \frac{ze^{-z}}{\sqrt{z^2-a^2}}\,\mathrm{d}z$$
$$= \sum_{n=0}^{\infty}(-2\pi)^n \sum_{m=0}^{n} \frac{\sinh\big((1+n-2m)t\big)}{m!(n-m)!(1+n-2m)}.$$

The incomplete Bessel representation in (23) provides a convenient form for numerical evaluation of the K-function.

Figure 4 shows the theoretical non separable Matérn covariance (20) (top row) and the corresponding pair correlation (21) (bottom row) functions for the same values of $(\alpha_s^{-1}, \alpha_t^{-1})$ used in the separable case. Relative to the separable Matérn model, the covariance surfaces exhibit sharper gradients, and the regions of repulsion in the pair correlation function are more compact for a given set of range parameters, reflecting the faster joint decay of dependence in the non separable case. Because spatial and temporal components interact through the combined metric $\sqrt{\alpha_t^2 t^2 + \alpha_s^2 \|u\|^2}$, changes in the temporal range affect spatial dependence and vice versa, producing a more localized and directionally varying pattern of inhibition. Figure 5 further highlights these contrasts under a set of larger range parameters $(\alpha_s^{-1}, \alpha_t^{-1})$, chosen to make the differences between the two structures more visually apparent.

In comparison of all three models, the Gaussian–Exponential model is suited to settings with smooth, mild inhibition (see Figure 2 and left panels in Figure 6); the separable Matérn model accommodates stronger, independently structured spatial and temporal inhibition (see Figure 3 and middle panels in Figure 6); and the non separable Matérn model is most

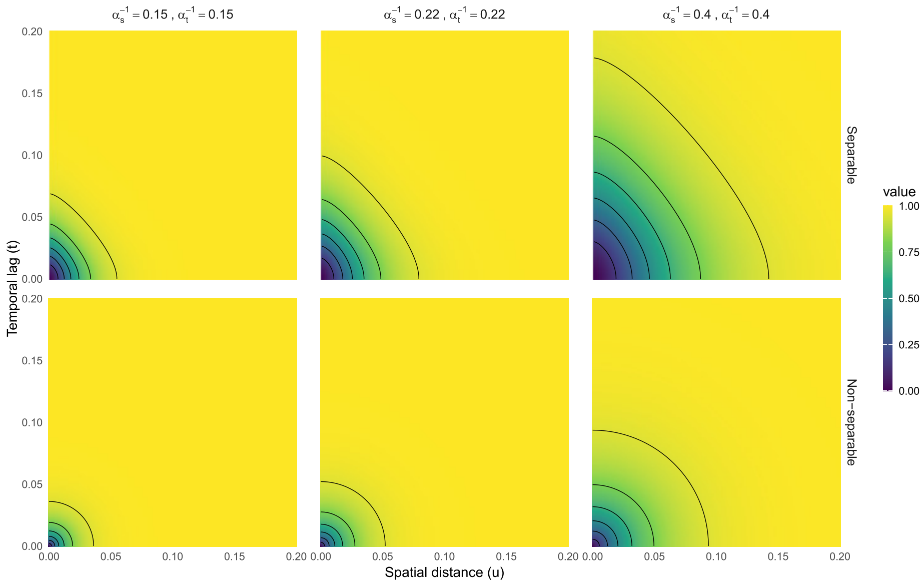

Figure 5. Pair correlation function for the separable (top row) and non separable (bottom row) **Matérn**stdpp models. Each column corresponds to a different combination of the parameters $(\alpha_s^{-1}, \alpha_t^{-1})$ selected according to the existence condition assuming $\rho_{\max} = 90$. This illustrates how increasing α_s^{-1} and α_t^{-1} broadens the effective interaction range and intensifies the repulsive behavior.

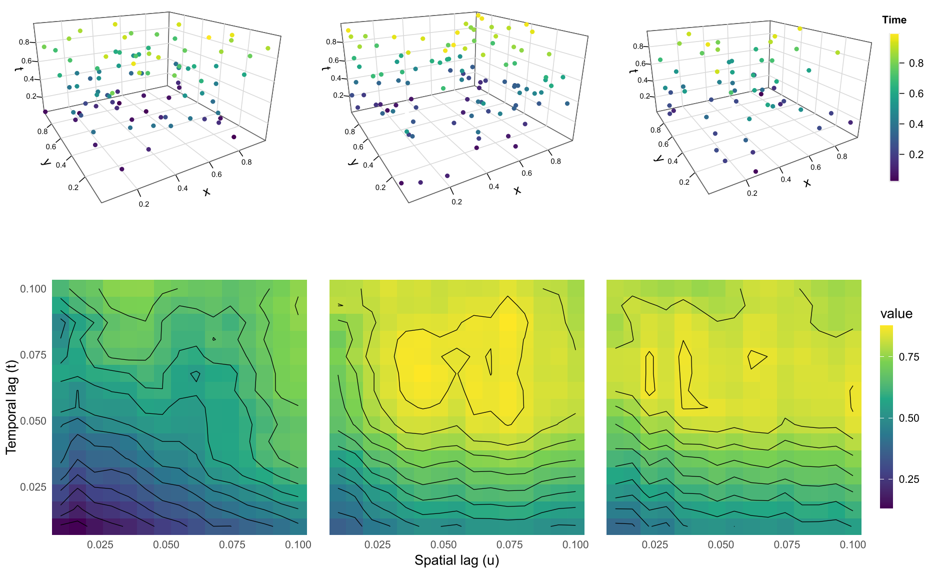

Figure 6. Top row: Illustrative realizations of stdpps with constant intensity $\rho = 90$, generated from three covariance models: Gaussian–exponential (left panels), separable Matérn (middle panels), and non separable Matérn (right panels). The simulations were performed on $[0,1]^2 \times [0,1]$ using parameter values $(\alpha_s, \alpha_t) = (0.12, 0.12)$ for model (i), and $(\alpha_s^{-1}, \alpha_t^{-1}) = (0.12, 0.12)$ for models (ii) and (iii). Bottom row: Estimated space-time pair correlation functions for the same models, averaged over 100 independent simulations.

Table 2. Summary of the Gaussian-exponential (first row), separable Matérn (second row), and non-separable Matérn (third row) spatio-temporal covariance models, along with their corresponding pair correlation functions, K-functions, and maximum admissible intensities $\rho_{\max}$.

$C_0(u,t)$	$g(u,t)$	$K(u,t)$	$\rho_{\max}$
$\rho\sigma_s^2\sigma_t^2 \exp\left(-\frac{\|u\|^2}{\alpha_s}-\frac{\|t\|}{\alpha_t}\right)$, Eq. (10)	$1-\exp\left(-\frac{2\|u\|^2}{\alpha_s}-\frac{2\|t\|}{\alpha_t}\right)$, Eq. (12)	Eq. (13)	$(2\pi\alpha_s^2\alpha_t)^{-1}$
$\gamma\pi^2(4\alpha_s^2\alpha_t^3)^{-1}(2\pi\alpha_t\|t\|+1)\times$ $\exp(-2\pi\alpha_t\|t\|)(2\pi\alpha_s\|u\|)\times$ $\mathcal{K}_1(2\pi\alpha_s\|u\|)$, Eq. (16)	$1-(2\pi\alpha_t\|t\|+1)^2\exp(-4\pi\alpha_t\|t\|)\times$ $\left[(2\pi\alpha_s\|u\|)\mathcal{K}_1(2\pi\alpha_s\|u\|)\right]^2$, Eq. (17)	Eq. (18)	$\pi^2\alpha_s^2\alpha_t/4$
$\gamma\pi^2(2\alpha_s^2\alpha_t^3)^{-1}\times$ $\exp\left(-2\pi\left(\alpha_t^2\|t\|^2+\alpha_s^2\|u\|^2\right)^{1/2}\right)$, Eq. (20)	$1-\exp\left(-4\pi\left(\alpha_t^2\|t\|^2+\alpha_s^2\|u\|^2\right)^{1/2}\right)$, Eq. (21)	Eq. (22)	$\pi^2\alpha_s^2\alpha_t/2$

appropriate when the data exhibit pronounced inhibition and essential space–time interaction (see Figure 4 and right panels in Figure 6).

Table 2 provides an overview of the spatio-temporal covariance models together with their corresponding first- and second-order characteristics discussed in Sections 3.2 and 3.3. Figure 7 illustrates the feasible parameter regions for the Gaussian–Exponential model (left), the separable Matérn model (middle), and the non separable Matérn model (right), derived from the respective existence conditions under a maximum intensity of $\rho = 90$. In each panel, the light green region denotes admissible parameter combinations, while the light red region indicates infeasible ones.

4. Simulation study for comparing covariance structures in stdpps

This section presents a simulation study designed to illustrate how alternative covariance structures shape the behavior of the proposed STDPP models. The aim is not to investigate first-order properties or to undertake parameter estimation, but rather to visualize and interpret how different kernel formulations–particularly the contrast between separable and non separable forms–influence the resulting space-time patterns and the strength of repulsion among events.

4.1. Simulation framework

We consider stationary and isotropic STDPPs defined on the unit space-time window $W \times T = [0,1]^2 \times [0,1]$ with constant intensity $\rho = 90$. Realizations are generated using an extension of the simulation algorithm of Lavancier et al. (2015), adapted to the spatio-temporal setting. This framework allows efficient generation of realizations with a prescribed kernel $C((u_1,t_1),(u_2,t_2))$. To simulate from an inhomogeneous STDPP, we follow the standard thinning strategy: a stationary process is generated at the maximal admissible intensity $\rho_{\max}$

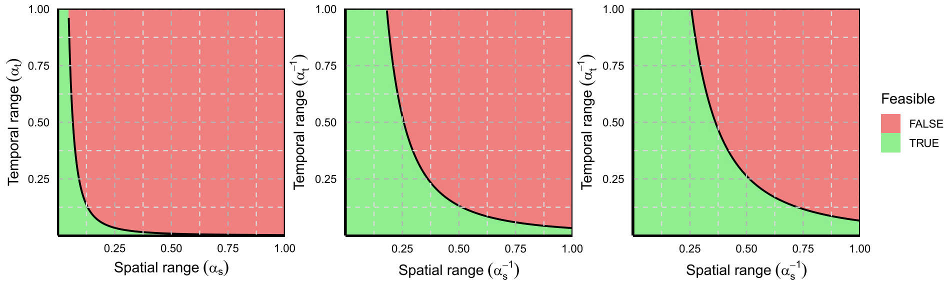

Figure 7. Feasible parameter regions for the Gaussian–Exponential stdpp model (left), the separable Matérn stdpp model (middle), and the non separable Matérn stdpp model (right) under a maximum intensity of $\rho = 90$. In each plot, the light green area displays the feasible parameter region, whereas the light red area shows infeasible parameter combinations.

and is then thinned independently with probability $p(u,t) = \frac{\rho(u,t)}{\rho_{\max}}$, where $\rho(u,t)$ denotes the desired intensity function. As shown in Lavancier et al. (2015), the resulting thinned process remains a STDPP. For details on simulating inhomogeneous STDPPs, see Appendix A in Ghorbani et al. (2025). In this study, we focus solely on the stationary case for clarity. All simulations were implemented in R, using routines adapted from the `spatstat` and `stpp` packages.

The simulation study examines three covariance models introduced in Section 3: (i) the separable Gaussian–exponential model, (ii) the separable Matérn model, and (iii) the non separable Matérn model. The admissible parameter regions for these models were derived in Sections 3.2 and 3.3 and are visualized in Figure 7. For illustrative purposes, and to enable direct comparison with the theoretical results in Section 3, we use the parameter values $(\alpha_s, \alpha_t) = (0.12, 0.12)$ for the Gaussian–exponential model, and $(\alpha_s^{-1}, \alpha_t^{-1}) = (0.12, 0.12)$ for both the separable and non separable Matérn models. Recall that for the Matérn models the parameters $(\alpha_s^{-1}, \alpha_t^{-1})$ represent the spatial and temporal *range* parameters, so larger values correspond to slower decay of dependence in space and time.

4.2. *Typical realizations and estimated pair correlation functions structure*

Figure 6 shows representative realizations and estimated space–time pair correlation functions $\hat{g}(u,t)$ averaged over 100 independent simulations. To estimate the space-time pair correlation function the function PCFhat in the R package `stpp` (Gabriel et al., 2024) has been used. The Gaussian-exponential STDPP model (left panels) yields smooth, moderately long-range repulsion with a separable structure in space and time. The separable Matérn STDPP model (middle panels) exhibits short-range inhibition with rapid and independent decays in its spatial and temporal components, consistent with the fast-decaying Matérn correlations in each dimension. The non separable Matérn STDPP model (Right panel) generates strong, localized around origin joint inhibition: events close in space tend to be separated in time, and vice versa. In other words, the separable Matérn exhibits independent spatial and temporal repulsion, producing evenly distributed points across layers, while the non separable model shows coupled space–time regularity, where nearby times correspond to stronger spatial repulsion. These differences reflect the theoretical behavior of the covariance

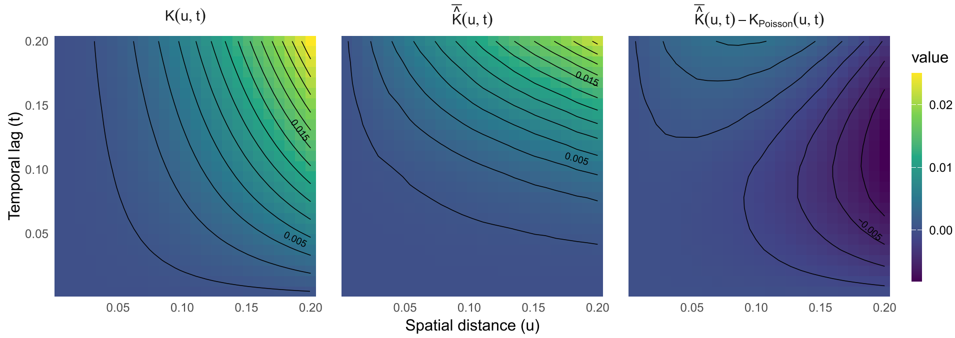

Figure 8. Theoretical K-function for the Gaussian-exponential stdpp model (left) with constant intensity $\rho = 90$ and $(\alpha_s, \alpha_t) = (0.12, 0.12)$, mean of $\hat{K}$s ($\bar{\hat{K}}$) based on 100 simulations of this model with the same parameter values on $[0,1]^2 \times [0,1]$ (middle), and $\bar{\hat{K}} - K_{Poisson}$ (right).

and pair correlation functions in Section 3, confirming that the covariance structure directly governs the spatial, temporal, and joint scales of repulsion.

Further, the estimated pair correlation functions satisfy $\hat{g}(u,t) \leq 1$, reflecting the intrinsic regularity of determinantal processes. Small discrepancies between the theoretical pair correlation functions (Figures 3 and 4) and their empirical estimates (Figure 6) arise from bandwidth selection, edge effects, and the well-known bias of kernel-based estimators at small space–time lags. Overall, the theoretical and empirical K-functions show close agreement (Figure 8), with $\bar{\hat{K}} - K_{\text{Poisson}}$ negative for most (u,t), consistent with regularity.

Overall, the simulation study demonstrates that the STDPP framework can reproduce a wide range of repulsive space–time patterns. Separable models offer interpretable and independently controlled spatial and temporal ranges, whereas non separable models provide stronger, jointly structured inhibition. These findings not only reinforce the theoretical developments presented in Section 3 but also provide practical guidance for selecting appropriate covariance models in applied settings.

5. Discussion and conclusion

In this work, we developed a general covariance-based framework for constructing *spatio-temporal determinantal point processes* (STDPPs) that flexibly model repulsive interactions across space and time. By extending classical spatial DPP theory to the spatio-temporal domain through valid covariance and spectral structures, we provided a unified treatment of separable and non separable STDPP models and derived closed-form expressions for key second-order characteristics, including the spatio-temporal pair correlation function and K-function. These results establish a principled foundation for modelling regularity in dynamic space–time phenomena.

The simulation study illustrates the practical implications of the theoretical developments, highlighting the distinct behaviors induced by different covariance structures. The Gaussian-exponential STDPP produces smooth, long-range inhibition with separable spatial and temporal dimensions. The separable Matérn STDPP allows independent control of spatial and temporal range parameters, yielding short-range inhibition that decays fast in each dimension. In contrast, the non separable Matérn STDPP induces stronger and more localized repulsion, reflecting its joint dependence on a combined space–time distance metric. The resulting realizations exhibit stronger and more localized repulsion, consistent with the faster decay of the non separable covariance. These qualitative differences demonstrate how the choice of covariance structure shapes the underlying dependence and underscores the importance of domain knowledge and exploratory analysis when selecting a model in practical application.

Statistical inference for STDPPs can build on the rapidly developing toolbox available for spatial DPPs. Likelihood-based and minimum-contrast approaches (Lavancier et al. 2015) extend naturally to the spatio-temporal setting, and composite likelihood methods (Lavancier et al. 2021) provide a scalable alternative for larger datasets. Model assessment can be performed using global envelope tests (Myllymäki et al. 2017). Nonetheless, several challenges remain. Kernel estimators of the spatio-temporal pair correlation function require joint bandwidth selection in space and time, and edge correction becomes more intricate in a cylindrical space–time window. These issues are evident in the simulation study: while theoretical and empirical K-functions generally agree (see Figure 8), the pair correlation estimator is sensitive to bandwidth choices at small lags. Establishing principled, data-adaptive smoothing strategies for space–time summary statistics is therefore an important topic for future work.

In comparison with other spatio-temporal point process models (Table 1), STDPPs occupy a unique position. Gibbs and Markov models accommodate repulsion but suffer from intractable normalizing constants and computationally intensive inference. Log-Gaussian Cox processes offer great flexibility and capture clustering, but cannot represent repulsion. STDPPs combine repulsiveness, model interpretability, and computational tractability through closed-form spectral and covariance representations and an exact thinning-based simulation algorithm. This makes STDPPs a compelling option for applications where regular, well-dispersed patterns arise, such as ecological dynamics, epidemiology, forestry, and environmental monitoring.

The proposed framework also has limitations that point to several avenues for further research. First, we focused on stationary and isotropic structures; extending STDPPs to non stationary or anisotropic domains would allow modelling of spatial heterogeneity, temporal trends, and directional effects. Second, computational scalability remains an important consideration: eigenvalue decompositions of large space–time kernels are expensive, and future work could leverage low-rank spectral approximations (Affandi et al. 2013; Affandi et al. 2014), sparse kernels, or inducing-point strategies. Third, comprehensive inferential tools–including parameter estimation, model selection, uncertainty quantification, and diagnostic tests–require additional development, especially for non separable structures with strong space–time interaction.

Overall, the covariance-based STDPP framework introduced here provides a flexible, interpretable, and computationally tractable foundation for modelling repulsive phenomena evolving across space and time. By linking covariance structure, spectral properties, and second-order characteristics, this work lays the groundwork for applying STDPPs to diverse scientific domains such as epidemiology, ecology, forestry, and environmental sciences, where understanding repulsiveness in space–time patterns is essential.

Acknowledgments

The authors would like to thank Frederic Lavancier and Ege Rubak for insightful discussions. They are also grateful to the anonymous referees and the associate editor for their constructive comments and suggestions, which greatly improved the manuscript.

Disclosure statement

No potential conflict of interest was reported by the author(s).

Funding

MG was financially supported by the Kempe Foundations (grant number JCSMK22-0134) and the Olle Engkvists Foundation (grant number 224-0071), NV by the Kempe Foundations (grant number JCSMK22-0134), and MM by the Academy of Finland (project numbers 295100 and 327211).

References

Abramowitz M, Stegun IA. 1992. Handbook of mathematical functions with formulas, graphs, and mathematical tables. Dover Publications Inc.

Adachi K. 2020. Matrix-based introduction to multivariate data analysis. Springer.

Affandi RH, Fox E, Adams R, Taskar B. 2014. Learning the parameters of determinantal point process kernels. In: Xing EP, Jebara T, editors. *Proceedings of the 31st International Conference on Machine Learning*; Vol. 32. PMLR. p 1224–1232.

Affandi RH, Fox EB, Taskar B. 2013. Approximate inference in continuous determinantal point processes, ArXiv abs/1311.2971,

Baddeley AJ, Møller J, Waagepetersen R. 2000. Non- and semi-parametric estimation of interaction in inhomogeneous point patterns. Stat Neerl. 54(3):329–350. doi: 10.1111/1467-9574.00144.

Bernabeu A, Zhuang J, Mateu J. 2024. Spatio-temporal Hawkes point processes: a review. J Agric Biol Environ Stat. 30:89–119.

Biscio CAN, Lavancier F, Waagepetersen RP. 2016. Parametric estimation for determinantal point processes. Scand J Stat. 43:999–1023.

Biscio CAN, Waagepetersen RP. 2019. A general framework for log-linear models of repulsive spatial point processes. Biometrika. 106:305–322.

Borodin A, Corwin I, Guionnet A. 2019. Random matrices IAS/Park City mathematics series. American Mathematical Society.

Cressie NAC. 1993. Statistics for spatial data, 2nd ed. Wiley.

Cressie N, Wikle CK. 2011. Statistics for spatio-temporal data. John Wiley and Sons.

Cronie O, Van Lieshout MNM. 2015. A J-function for Inhomogeneous spatio-temporal point processes. Scand J Stat. 42(2):562–579. doi: 10.1111/sjos.12123.

Daley D J, Vere-Jones D. 2008. An introduction to the theory of point processes general theory and structure, 2nd ed. II. Springer-Verlag.

Diggle P. 2007. Spatio-temporal point processes: methods and applications. In: Finkenstädt B, Held L, Isham V, editors. Statistical methods for spatio-temporal systems. Chapman and Hall/CRC. p 1–45.

Diggle PJ. 2013. Statistical analysis of spatial and spatio-temporal point patterns. Chapman and Hall/CRC.

Fuentes M, Chen L, Davis JM. 2008. A class of nonseparable and nonstationary spatial temporal covariance functions. Environmetrics. 19(5):487–507. doi: 10.1002/env.891.

Gabriel E. 2014. Estimating second-order characteristics of inhomogeneous spatio-temporal point processes. Methodol Comput Appl Probab. 16(2):411–431. doi: 10.1007/s11009-013-9358-3.

Gabriel E, Diggle PJ. 2009. Second-order analysis of inhomogeneous spatio-temporal point process data. Stat Neerl. 63(1):43–51. doi: 10.1111/j.1467-9574.2008.00407.x.

Gabriel E, Diggle PJ, Rowlingson B, Rodriguez-Cortes FJ. 2024. *stpp: Space-time point pattern simulation, visualisation and analysis*, R package version 2.0-8 [Software], https://CRAN.R-project.org/package=stpp.
Ghorbani M. 2013. Testing the weak stationarity of a spatio-temporal point process. Stoch Environ Res Risk Assess. 27(2):517–524. doi: 10.1007/s00477-012-0597-6.
Ghorbani M, Vafaei N, Myllymäki M. 2025. A kernel-based test for the first-order separability of spatio-temporal point processes. TEST. 34:580–611.
Gonzalez JA, Hahn U, Mateu J. 2019. Analysis of tornado reports through replicated spatio temporal point patterns. Jo Royal Statist Soc Ser C. 69:1–21.
González JA, Rodríguez-Cortés FJ, Cronie O, Mateu J. 2016. Spatio-temporal point process statistics: A review. Spat Stat. 18:505–544. doi: 10.1016/j.spasta.2016.10.002.
Gradshteyn I S, Ryzhik I M. 2007. Table of integrals, series, and products, 7th ed. Academic Press.
Horn RA, Johnson CR. 2013. Matrix analysis, 2nd ed. Cambridge University Press.
Iftimi A, Cronie O, Montes F. 2019. Second-order analysis of marked inhomogeneous spatiotemporal point processes: Applications to earthquake data. Scandinavian J Statistics. 46(3):661–685. doi: 10.1111/sjos.12367.
Illian J, Penttinen A, Stoyan H, Stoyan D. 2008. Statistical analysis and modelling of spatial point patterns. John Wiley and Sons.
Jones D S. 2007. Incomplete Bessel functions. I. Proc Edinburgh Math Soc. 50(1):173–183. doi: 10.1017/S0013091505000490.
Kulesza A, Taskar B. 2012. Determinantal point processes for machine learning. FoundTrends Mach Learn. 5(2-3):123–286. doi: 10.1561/2200000044.
Lavancier F, Møller J, Rubak E. 2015. Determinantal point process models and statistical inference. J Royal Statist Soc Ser B: Statist Methodol. 77(4):853–877. doi: 10.1111/rssb.12096.
Lavancier F, Møller J, Rubak E. 2022. Composite likelihood inference for determinantal point processes. J Ser B: Statist Methodol. Royal Statist So. 84:249–273.
Lavancier F, Poinas A, Waagepetersen R. 2021. Adaptive estimating function inference for nonstationary determinantal point processes. Scandinavian J Statistics. 48(1):87–107. doi: 10.1111/sjos.12440.
Lieshout MNM. 2000. Markov point processes and their applications. Imperial College Press.
Van Lieshout MNM, Baddeley A J. 1996. A nonparametric measure of spatial interaction in point patterns. Stat Neerl. 50(3):344–361. doi: 10.1111/j.1467-9574.1996.tb01501.x.
Macchi O. 1975. The coincidence approach to stochastic point processes. Advances in Applied Probab. 7:83–122.
Matérn B. 1960. Spatial variation: stochastic models and their applications to problems in forest surveys and other sampling investigation. Meddelanden fraan Statens Skogforskningsinstitut Band 49, Nr 5, 144 p.
Meyer S, Elias J, Höhle M. 2012. A space-time conditional intensity model for invasive meningococcal disease occurrence. Biometrics. 68(2):607–616. doi: 10.1111/j.1541-0420.2011.01684.x.21981412
Møller J, Biscio CAN, Waagepetersen R P. 2023. Determinantal point process models for spatial data: a review and recent developments. Spat Stat. 56:100776.
Møller J, Ghorbani M. 2012. Aspects of second-order analysis of structured inhomogeneous spatio-temporal point processes. Stat Neerl. 66(4):472–491. doi: 10.1111/j.1467-9574.2012.00526.x.
Møller J, Syversveen AR, Waagepetersen RP. 1998. Log Gaussian cox processes. Scand J Stat. 25(3):451–482. doi: 10.1111/1467-9469.00115.
Møller J, Waagepetersen RP. 2004. Statistical inference and simulation for spatial point processes. Chapman and Hall/CRC.
Møller J, Waagepetersen RP. 2007. Modern statistics for spatial point processes*. Scand J Stat. 34(4):643–684. doi: 10.1111/j.1467-9469.2007.00569.x.
Myllymäki M, Mrkvička T, Grabarnik P, Seijo H, Hahn U. 2017. Global envelope tests for spatial processes. J Ser B (Statist Methodol). Royal Statist Soc. 79(2):381–404.
Ogata Y. 1998. Space-time point-process models for earthquake occurrences. Ann Inst Statist Math. 50(2):379–402. doi: 10.1023/A:1003403601725.
Rasmussen C E, Williams CKI. 2006. Gaussian processes for machine learning. The MIT Press.

Seaton FM, Jarvis SG, Henrys PA. 2024. Spatio-temporal data integration for species distribution modelling in R-INLA. Methods Ecol Evol. 15(7):1221–1232. doi: 10.1111/2041-210X.14356.

Soriano-Redondo A et al. 2019. Understanding species distribution in dynamic populations: a new approach using spatio-temporal point process models. Ecography. 42: 1092–1102. https://api.semanticscholar.org/CorpusID.

Strang G. 2006. Linear algebra and its applications, 4th ed. Thomson. Brooks/Cole.

Yang ZH, Chu YM. 2017. On approximating the modified bessel function of the second kind. J Inequal Appls. 2017:41.